



Journal of Mining and Environment (JME)

journal homepage: www.jme.shahroodut.ac.ir



THOMSON
REUTERS



Experimental Studies, Response Surface Methodology and Molecular Modeling for Optimization and Mechanism Analysis of Methylene Blue Dye Removal by Different Clays

Kumars Seifpanahi Shabani * and Babak Abedi Orang

Faculty of Mining, Petroleum and Geophysics Engineering, Shahrood University of Technology, Shahrood, Iran

Article Info

Received 22 July 2020

Received in Revised form 19
September 2020

Accepted 19 September 2020

Published online 5 October 2020

DOI: [10.22044/jme.2020.9916.1919](https://doi.org/10.22044/jme.2020.9916.1919)

Keywords

Adsorption Process

Methylene Blue

Response Surface

Molecular Modeling

Abstract

In this work, three types of natural clays including kaolinite, montmorillonite, and illite with different molecular structures, as adsorbents, are selected for the removal of methylene blue dye, and their performance is investigated. Also the optimization and the analysis of the dye adsorption mechanism are performed using the response surface methodology, molecular modeling, and experimental studies. The response surface optimization results demonstrate that the parameters affecting on the dye adsorption process are somewhat similar in all the three types of clays, and any difference in the impacts of the different parameters involved depends on the different structures of these three types of clays. The results of the experimental studies show that all the three clays follow the Temkin isotherm, and the comparison of the clay adsorption capacity is illite (3.28) > kaolinite (4.15) > montmorillonite (4.5) L/g. On the other hand, the results obtained from the laboratory studies and the response surface optimization were obtained using molecular modeling with the Gaussian and Chem-Office softwares. The results of these achievements confirm that the number of acceptor hydrogen bonds around the clays influence the adsorption capacity of methylene blue. Based on the results obtained, most adsorption capacities of clays are related to illite > kaolinite > montmorillonite that have 24, 18, and 16 acceptor hydrogens, respectively. The assessment of the adsorption mechanism process by the different methods confirms the dominance of the physical adsorption process and a minor effect of the chemical adsorption.

1. Introduction

Fresh or clean water is essential for life on the earth. The prerequisite for a sustainable development is the existence of a healthy water. The industrial and agricultural activities can be considered as the major pollutant sources for water resources and natural ecosystems [1, 2]. One of the most important groups of environmental pollutants can be dyes, many of which are present in the industrial effluents [3]. Dyes and pigments are widely used in the industries such as plastics, textiles, cosmetics, pharmaceuticals, and paper making [4, 5].

The recent studies have shown that more than 15% of the total amount of the dyes produced each

year is processed into the industrial effluents and converted into environmental pollutants during the production process [6, 7]. In addition to help the ecosystem, removing these pollutants can also have important economic benefits. Different biological and physico-chemical methods can be used to remove dyes from aquatic sources [2, 8 and 9]. Most of these methods have been performed only in the laboratory studies and at industrial levels; there are wide application limitations with them such as the cost of the method, high energy consumption, and operating time, and in some cases, the creation of secondary pulp that the pulp itself is required to be treated [10].

✉ Corresponding author: seifpanahi@shahroodut.ac.ir (K. Seifpanahi Shabani).

Therefore, the researchers are always looking for a simple and affordable solution to remove dyes from contaminated wastewaters [11]. Thus different biological and physico-chemical methods have been used to remove dyes from water sources in the recent years [12]. The chemical precipitation [13], sonochemical degradation [14], ultra-filtration [15], electrochemical treatment [16], solar photo-Fenton mechanisms [17], reverse osmosis [18], and adsorption process [19] are some methods that have been applied for dye removal.

Unlike the other methods, adsorption can be considered as a promising alternative method to remove dyes from water sources [10, 20 and 21]. However, all of these benefits are closely linked to the adsorbent used in the dye adsorption process. As a matter of fact, choosing an available and inexpensive adsorbent can be a great advantage for this process [22, 23]. Clays are the main sources used as adsorbents in the processing and environmental processes, and have always been regarded as the affordable and efficient adsorbents [24].

In this work, three clays from three main clay categories were selected as the adsorbents, and the methylene blue adsorption laboratory experiments on these adsorbent were performed. The adsorption efficiency of each adsorbent was determined by the adsorption isotherm, and the highest adsorption rate was predicted using the Design Expert 7 software. Finally, it was attempted to determine a reasonable relation between the adsorbent structures by molecular modeling and its efficiency.

In this work, using molecular modeling, the mechanism governing the adsorption of methylene blue by three natural clay adsorbents (kaolinite, illite, montmorillonite) was evaluated, and the results obtained were assessed and validated using the results of the batch experiments. For this aim, the Gaussian and chem3D software were used.

2. Materials and Method

Methylene blue (MB) (with the characterizations including the color index number: 52015, CAS number: 122965-43-9, empirical formula: $C_{16}H_{18}ClN_3S \cdot xH_2O$) was obtained from the Sigma Aldrich Company. At first, 100 mg of MB was dissolved in 1 L of distilled water to obtain 100 mg L^{-1} of a stock solution of the dye. Other concentrations of the dye solution were obtained from this solution. All the adsorbents were obtained from the Iran clay mines. In order to prepare the clay particles, three clay samples were

placed in a dryer at 105 °C to remove the water contained in them, and then they were cooled to room temperature, and finally, passed through a 2-mm sieve. The NaOH and HCl solutions used to adjust the pH were obtained from the Merck Company.

A Perkin Elmer Lambda 25 spectrophotometer was used for measurement of the dye concentrations. Phase separation was performed by a HERMLE centrifuge. The samples were mixed on a magnetic stirrer at 500 rpm. The pH variety was measured using a digital pH-meter. Scanning electron microscopy (SEM) was used to observe the adsorbent's morphology. The FT-IR spectra of the clays before and after the adsorption process were obtained between 450 cm^{-1} and 4000 cm^{-1} using a Perkin-Elmer spectrometer.

In the batch systems, the influence of some parameters like pH, concentration of contaminant, contact time, temperature, and adsorbent's dosage for the MB dye adsorption process was investigated and optimized. For the parametric optimization, the value for one parameter was changed and the other parameters were kept constant.

3. Results and Discussion

3.1. pH

At first, a solution of 100 ppm MB was prepared in doubly distilled water. Next, the adsorbents were added to the simulated wastewater solution and mixed at the pre-determined constant times of 10, 20, 40, 60, 80, 100, and 120 min using a magnetic stirrer at 500 rpm. At these times, the adsorbent was separated from the mixture using a centrifuge at about 4500 rpm, and the residual liquid was evaluated by the spectrophotometer for the amount of MB removed. The results obtained, which showed the adsorption percentage, were obtained by means of Equation 1.

$$R\% = (C_0 - C_e) \times 100 / C_0 \quad (1)$$

Where C_0 and C_e are the initial and final concentrations, respectively.

In order to determine the optimum pH of the adsorption for each adsorbent, at the pH values of 2, 3, 4, 5.5, and 7, the adsorption operations were performed at specified times, and the optimum pH value was determined for each adsorbent.

In all of these operations, the temperature was 25 °C, the initial dye concentration in the solution was 100 ppm, and the amount of adsorbent was 0.5 g. The optimization results for the pH for the adsorption of MB by kaolinite, illite, and

montmorillonite are shown in Figure 1. According to this figure, the optimum pH value for the adsorption of MB with the three adsorbents was set to 2. The effect of pH variation on the adsorption decreased at pH 4.

3.2. Pollutant concentration

In order to optimize the pollutant concentration, the 25 °C temperature, 500 rpm for the stirrer, 4500 rpm for centrifuge, 0.5 g for the amount of adsorbent, and the optimized pH value were used. The optimization diagrams For the MB concentration are given in Figure 2.

As shown in this figure, when the concentration of the contaminant was 50 ppm, the experiments with the three adsorbents showed the highest removal rates. When the concentration of the contaminant increased from 50 ppm to 100 ppm, the amount of adsorption was slightly reduced. However, by increasing the concentration to 150 ppm and 200 ppm, the adsorption decreased significantly. This decrease was offset by increasing the time to some extent but at low mixing times, the difference between adsorptions was more significant for the three adsorbents.

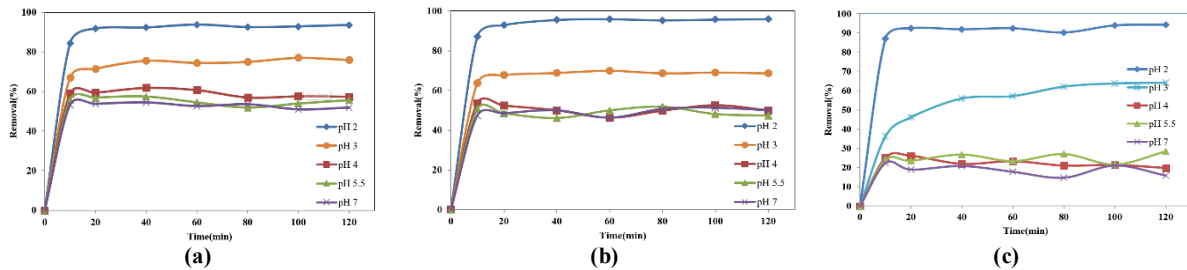


Figure 1. Optimization of pH for MB adsorption by a: kaolinite, b: illite, and c: montmorillonite.

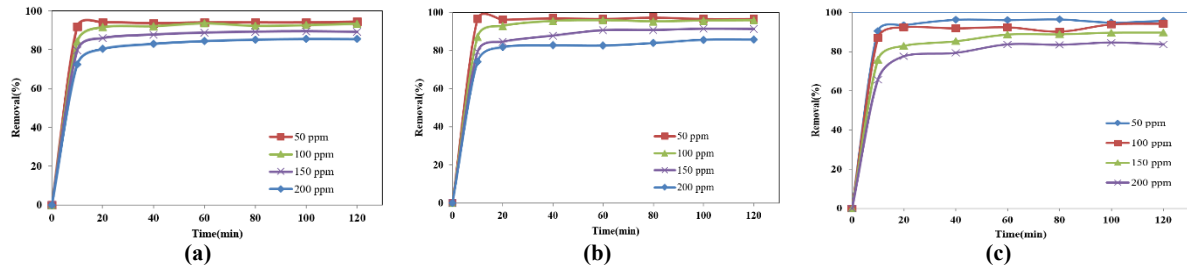


Figure 2. Optimization of MB concentration at optimum pH by a: kaolinite, b: illite, and C: montmorillonite.

3.3. Adsorbent dosage

By determining the optimum pH and the concentration of the contaminant, the dependence of the adsorption process on the weight of all the three adsorbents was evaluated. In order to optimize the weight of the adsorbent, the 25 °C temperature, 500 rpm for the stirrer, 4500 rpm for centrifuge, and the optimized pH were used. The effect of the weight of the adsorbent on the MB removal is shown in Figure 3 for the three adsorbents. The adsorbent amounts of 0.1, 0.2, 0.3, 0.4, and 0.5 g were used to remove MB. For all the three adsorbents, the removal rate improved with increase in the adsorbent content, and eventually, 0.5 g was determined as the optimum weight of the adsorbent. Also the adsorption performance at low

doses was improved at larger time intervals. In fact, by increasing the adsorption time for the three adsorbents, especially kaolinite and montmorillonite, the decrease in the amount of adsorbent was partially offset.

3.4. Temperature

In an adsorption, the adsorption temperature is an effective parameter. In order to optimize the adsorption temperature, a solution with 100 ppm concentration of the contaminant, 500 rpm for the stirrer, and 4500 rpm centrifuge were used at the optimum pH and weight of the adsorbent. Figure 4 shows the optimum adsorption temperature for the kaolinite, illite, and montmorillonite adsorbents.

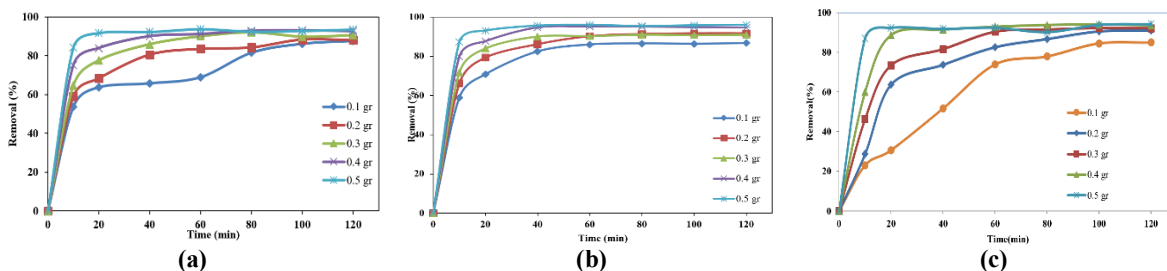


Figure 3. Optimizing weight of adsorbent. a: kaolinite, b: illite, and c: montmorillonite.

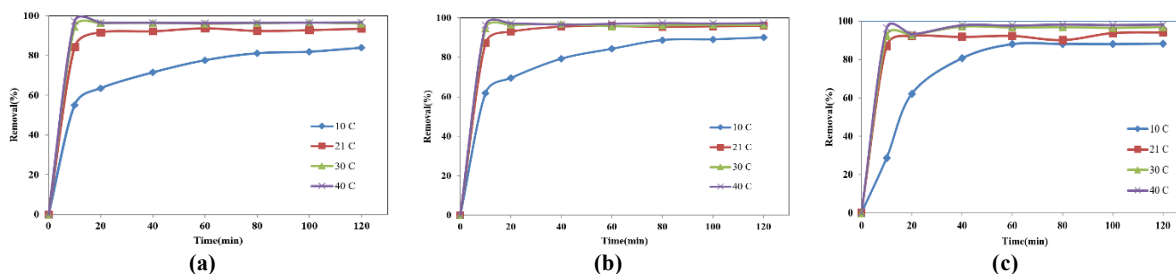


Figure 4. Optimization of adsorption temperature by the adsorbents a: kaolinite, b: illite, and c: montmorillonite.

As it can be seen in this figure, increasing the temperature from 10 °C to 21 °C has a significant effect on the adsorption rate. When the temperature of the solution reaches 21 °C, the slope of the influence of the temperature on the adsorption rate is reduced. Thus the effect of the adsorption temperature between the two temperatures of 30 °C and 40 °C can be ignored except for 10 min. In fact, it is expected that a temperature rise of 40 °C will not have much effect on the adsorption rate. It is also evident in the temperature studies that if the adsorption temperature is low, increasing the mixing time can partially increase the rate of the dye removal. However, at temperatures above 21 °C, the solution reaches equilibrium after 10 minutes. As a result, increasing the temperature accelerates and improves the adsorption process with the clay adsorbent. This effect is greater for montmorillonite than the other two adsorbents.

3.5. Statistical analysis

New spatial interpolation methods like machine learning methods and response surface for predicting the results and analyzing the mechanisms in problems have been considered in the recent years. The response surface methodology was used to predict as well as determining the interaction of the operational parameters in the Expert Design software. Also it was used to optimize the variables, although in this work, the experimental data was analyzed with the historical data part by this software. The Expert

Design software was used to determine the role of every operational parameter in the MB removal. Fig. 5 illustrates the interaction of the operating parameters in the MB removal.

Figures 5a-5c show that in all the three adsorbents, from pH 7 to pH 4, no noticeable change in the adsorption rate was observed but from pH 4 to pH 2, there was a sharp change, indicating that with increasing acidity, the disturbing factors such as OH decreased and their competition with the dye for binding to the adsorption sites was diminished. Figures 5d-5i, on the other hand, show that the interaction of time and pH follows a parabolic function. In fact, at a constant pH value, the adsorption process is increased till approximately 70 minutes as a parabolic function, reaching the highest removal rate at every pH. It is evident that after achieving the highest adsorption and occupancy of most adsorption sites, continued mixing has caused the adsorbed dye to be separated again. It can be concluded that the bonds formed lack a sufficient attraction, and we can consider them as physical bonds. The figure also shows the slight influence of temperature on the amount of adsorption at different times. In fact, time is a determining factor in the absorption of dyes in comparison to temperature because the graph shows that temperature at a given time has little effect on the absorption rate. This confirms the physicality of the adsorption process.

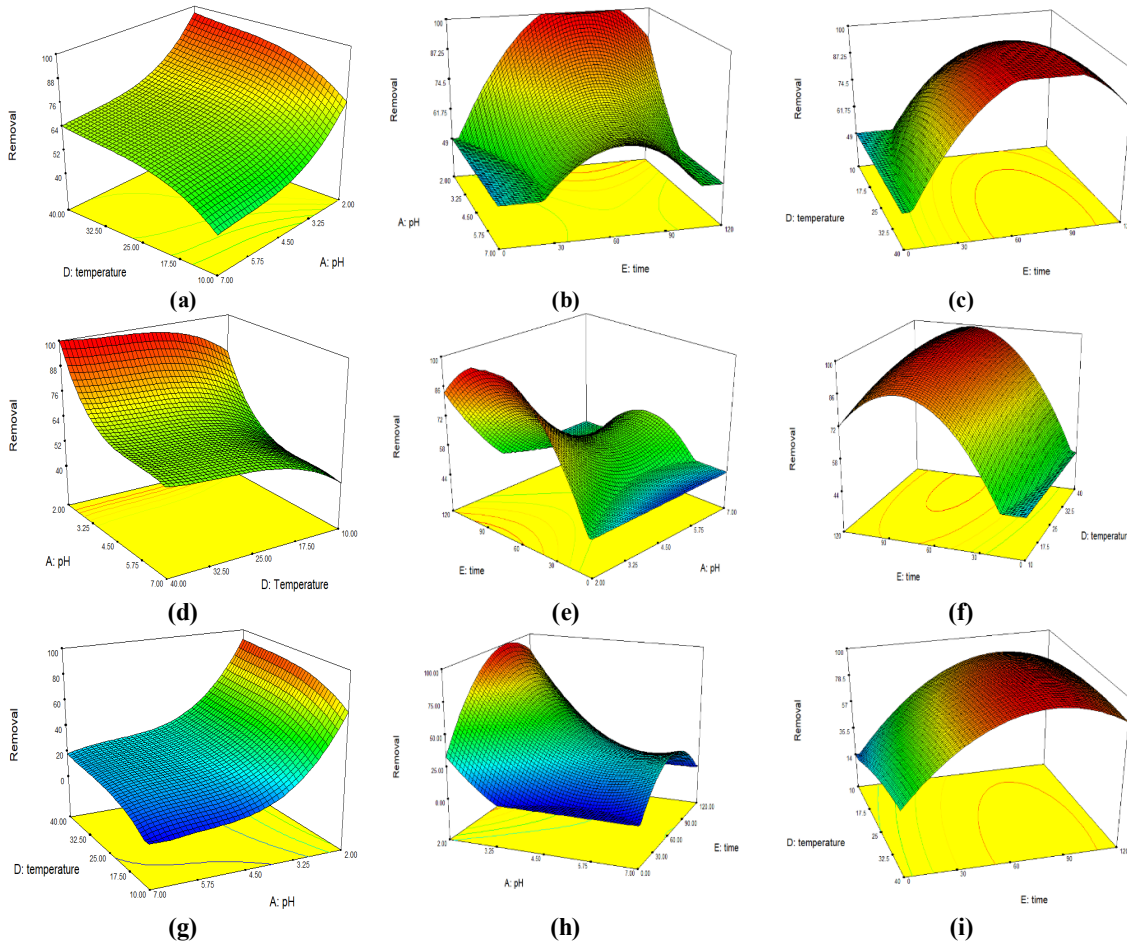


Figure 5. 3D surface mapping plots. a, b, c: temperature and pH; d, e, f: temperature and time; g, h, i: pH and time for MB adsorption by kaolinite, illite, and montmorillonite, respectively.

3.6. Adsorption isotherm

The adsorption isotherm provides valuable information regarding the adsorption optimization. The degree of affinity between the dye and the adsorbent, the bond energy, and the adsorption capacity can be calculated by means of the

adsorption isotherms [25]. Therefore, in this work, the Langmuir, Freundlich, and Temkin isotherms were investigated for the adsorption process with the three adsorbents. The equations of the Langmuir, Freundlich, and Temkin isotherms are given in Table 1.

Table 1. Isotherm models and their linear form [26]

Isotherm type	Equation	Linear form
Langmuir	$q_e = \frac{q_m K_L C_e}{1 + K_L C_e}$	$\frac{C_e}{q_e} = \frac{1}{K_L q_m} + \frac{1}{q_m} C_e$
Freundlich	$q_e = K_F C_e^{\frac{1}{n}}$	$\ln(q_e) = \ln K_F + \frac{1}{n} C_e$
Temkin	$q_e = \frac{RT}{b} \ln(K_T C_e)$	$q_e = \frac{RT}{b} \ln K_T + \frac{RT}{b} \ln C_e$

In this table, q_e (mg/g) and C_e (mg/L) are the amounts of the adsorbed dye per unit mass of the adsorbent and the dye concentration at equilibrium, respectively, q_m (mg/g) is the maximum amount of dye per unit mass of adsorbent to form a complete

monolayer on the surface, K_L (mg/L) is a constant related to the affinity of the binding sites, K_F and $1/n$ are the Freundlich constants, indicating the capacity and intensity of the adsorption, respectively, b (J/mol) is the Temkin constant that

is related to the heat of adsorption, and K_T (L/g) is the Temkin isotherm constant.

According to the laboratory data and the equations in Table 1, the Langmuir, Freundlich,

and Temkin isotherm results are shown in Figures 6 to 8 for the kaolinite, illite, and montmorillonite adsorbents, respectively. According to these Figures, the MB adsorption process for all the three adsorbents follows the Temkin isotherm.

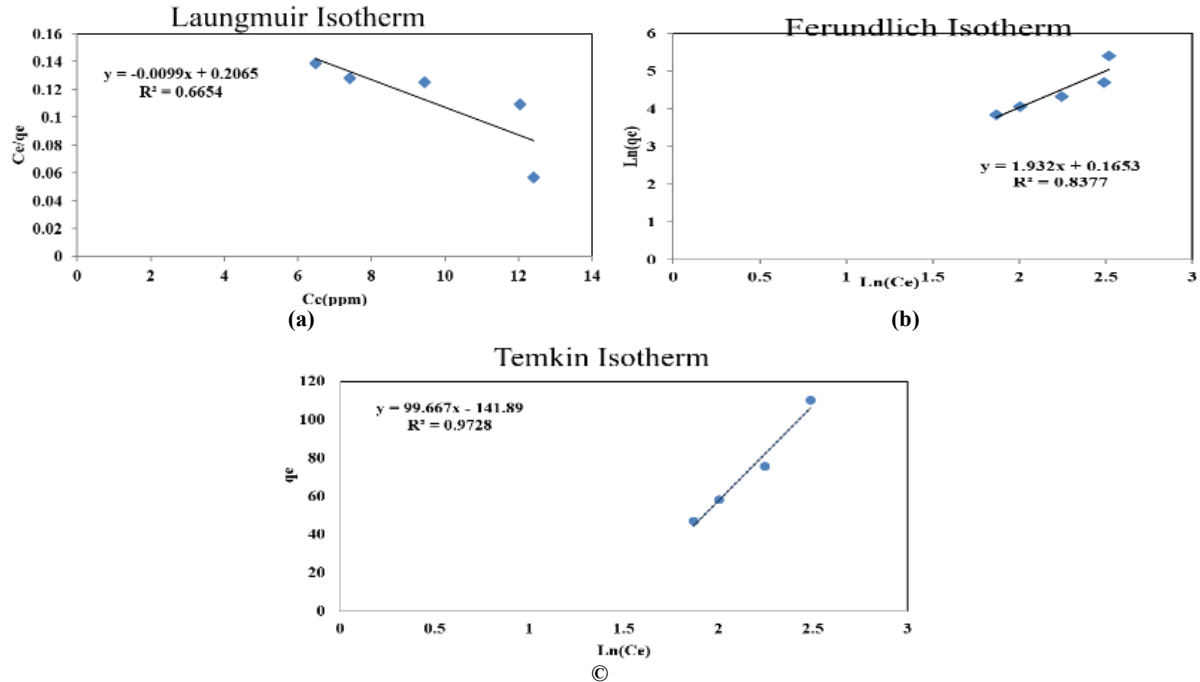


Figure 6. Linear fitting of the Langmuir (a), Freundlich (b), and Temkin (c) isotherms for the adsorption of MB by kaolinite.

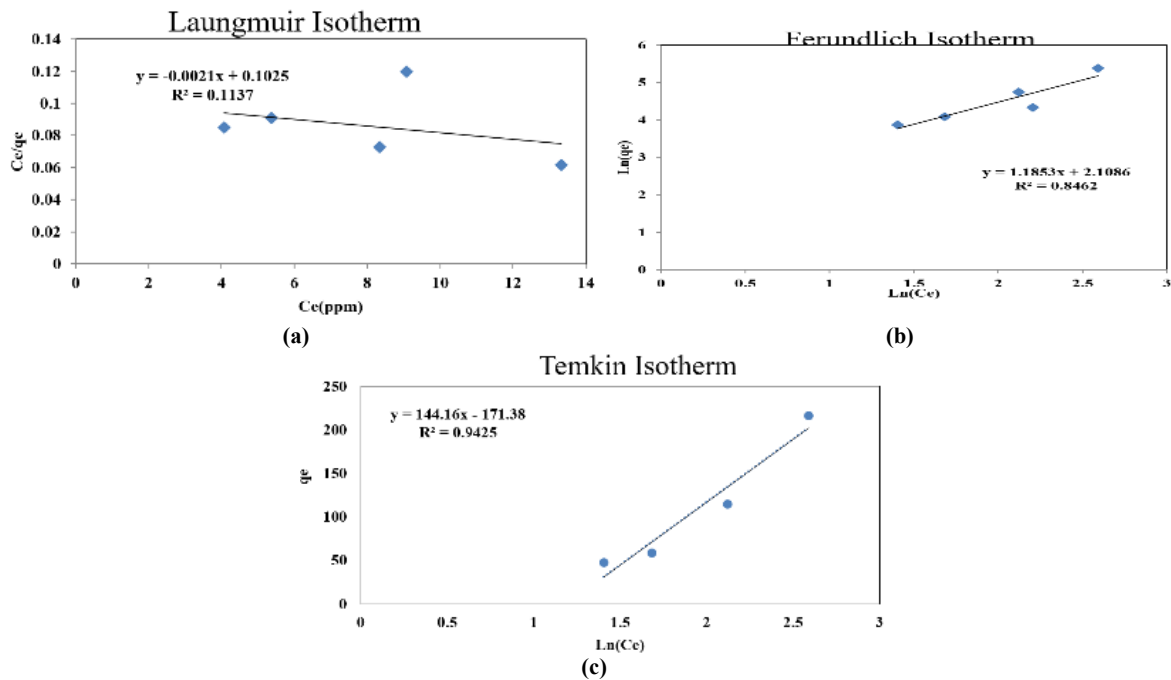


Figure 7. Linear fitting of the Langmuir (a), Freundlich (b), and Temkin (c) isotherms for the adsorption of MB by illite.

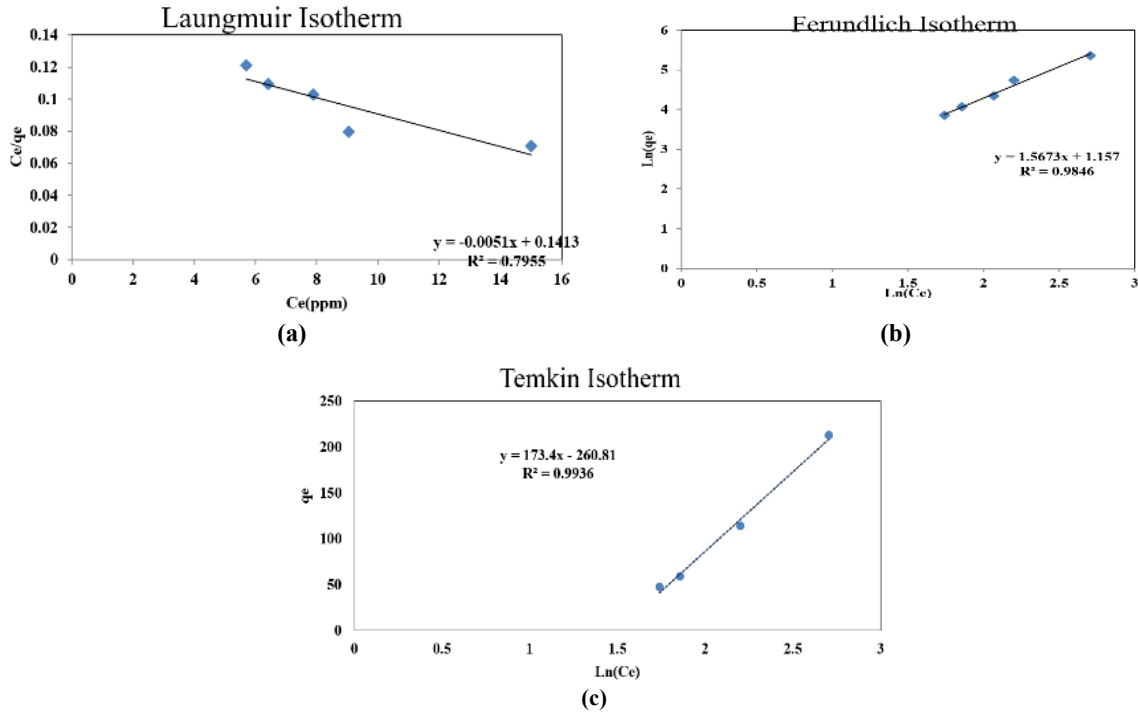


Figure 8. Linear fitting of the Langmuir (a), Freundlich, (b) and Temkin (c) isotherms for the adsorption of MB by montmorillonite.

3.7. Adsorption kinetics

The mechanism and rate of MB adsorption were investigated using the pseudo-first-order kinetics, pseudo-second-order kinetics, and intra-particle diffusion model. These equations are presented in Table 2.

In Table 2, q_e (mg/g) and q_t (mg/g) are the adsorption capacities of MB at equilibrium and at

time t , respectively; k_1 (min^{-1}), k_2 ($g(mg \cdot \text{min})^{-1}$), and k_{int} ($\text{L} \cdot \text{min}^{1/2}$) are the pseudo-first-order rate constant, pseudo-second-order rate constant, and intra-particle diffusion rate constant, respectively; and t indicates the equilibrium time. According to the laboratory data and Table 2, the results for the kinetics are shown in Figures 9-11.

Table 2. Equations of kinetic models with a linear equation [26].

Kinetic Model	Equation	Linear Equation
pseudo-first-order	$\frac{dq_t}{dt} = k_1(q_e - q_t)$	$\ln(q_t - q_e) = \ln q_e - k_1 t$
pseudo-second-order	$\frac{dq_t}{dt} = k_2(q_e - q_t)^2$	$\frac{t}{q_t} = \frac{1}{k_2 q_e^2} + \frac{1}{q_e} t$
Intra-particle diffusion	$q_t = K_{\text{int}} t^{(0.5)}$	$q_t = K_{\text{int}} t^{(0.5)}$

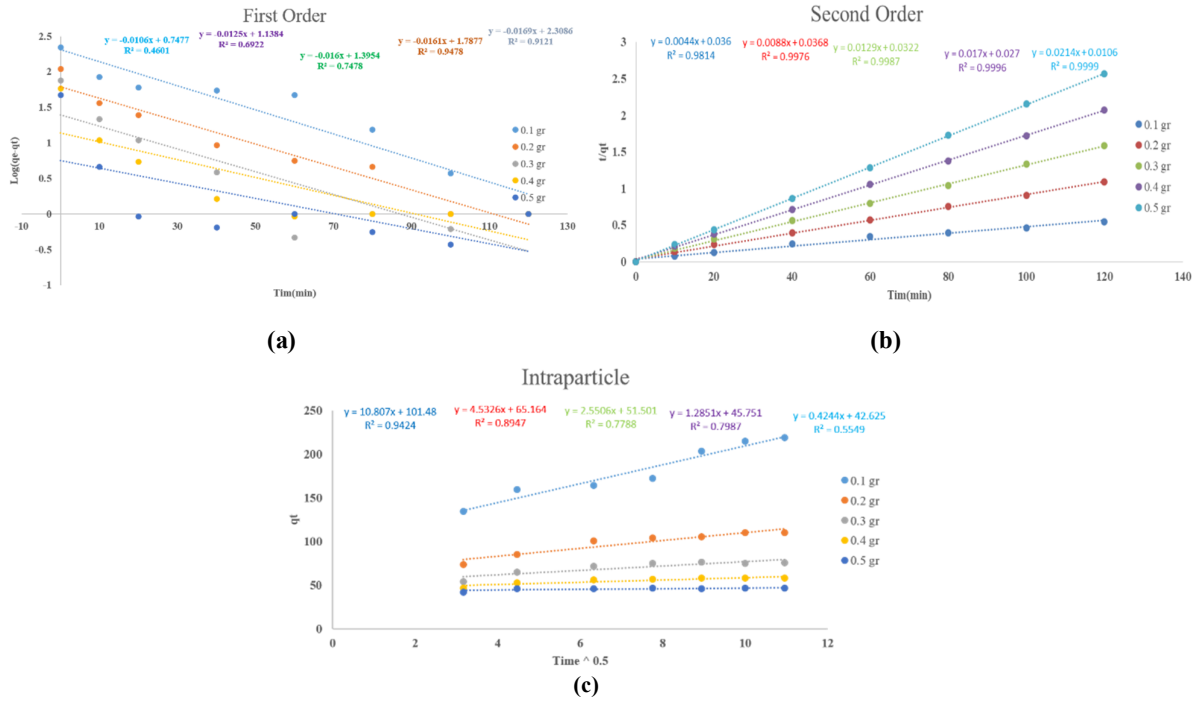


Figure 9. Kinetics of pseudo-first-order (a), pseudo-second-order (b), and intra-particle diffusion (c), and their linear fit for adsorption of MB by kaolinite with a variable amount of adsorbent.

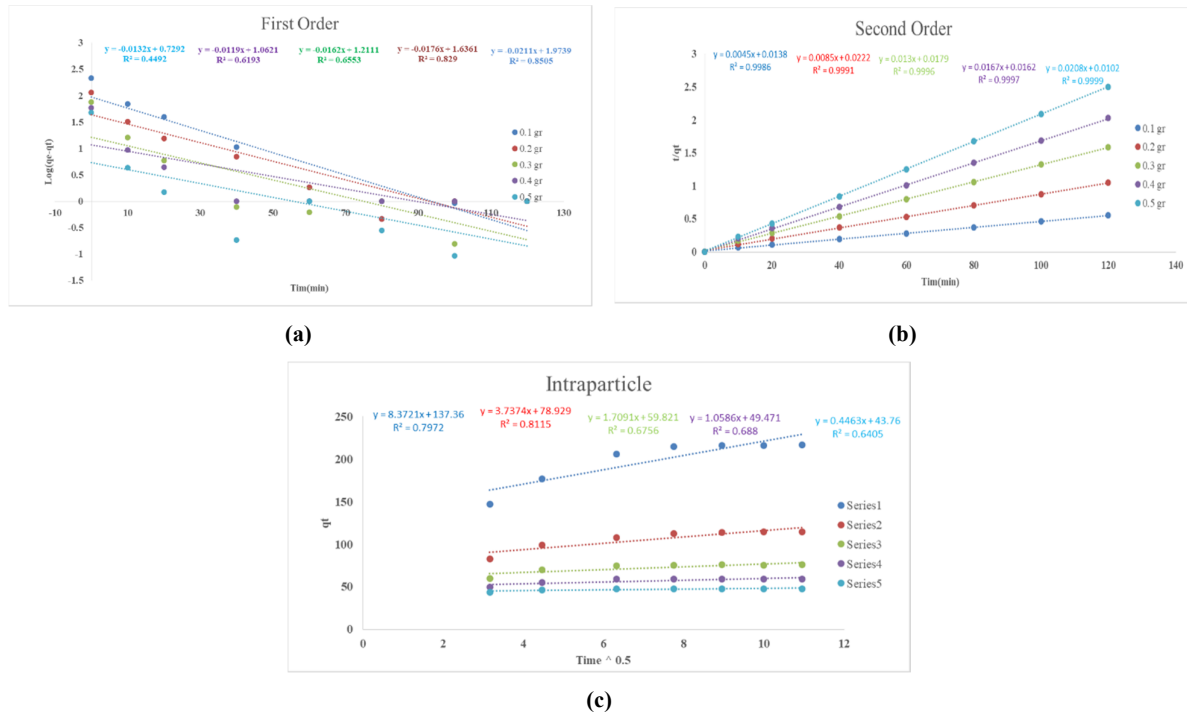


Figure 10. Kinetics of pseudo-first-order (a), pseudo-second-order (b), and intra-particle diffusion (c), and their linear fit for adsorption of MB by illite with a variable amount of adsorbent.

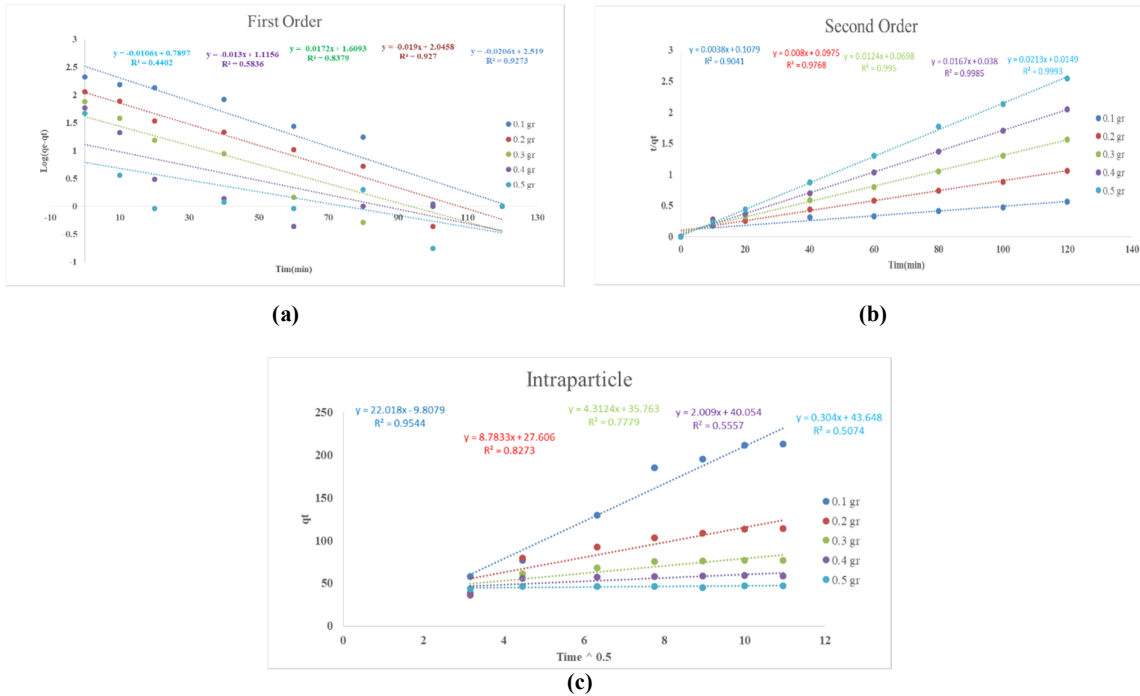


Figure 11. Kinetics of pseudo-first-order (a), pseudo-second-order (b), and intra-particle diffusion (c), and their linear fit for adsorption of MB by montmorillonite with a variable amount of adsorbent.

Using the linear fit of the laboratory data shown in Figures 11 to 13, the kinetic and adsorption parameters were obtained at equilibrium. The linear fit of the kinetic models for the 0.1, 0.2, 0.3, 0.4, and 0.5 adsorbent values is presented in Table 3.

According to Table 3, it is proved that the MB adsorption process in all cases follows the pseudo-second-order kinetics because it is most correlated with the laboratory data. It can be concluded that all the three selected clays exhibit similar kinetic

behaviors for adsorption of MB. The high correlation coefficient and the high value of matching of the laboratory data and the calculated data for q_e of the linear fit indicate that the adsorption process follows the pseudo-second-order kinetics. The adsorption kinetics are carried out in three steps, as shown in Figure 12, and it includes the transfer of soluble pollutants to the solid particle surface and intra-particle diffusion, and stay on the active adsorption sites [28].

Table 3. Linear fit of the kinetic model parameters.

Adsorbent	Linear fit for adsorption kinetic		
	pseudo-first-order	pseudo-second-order	intra-particle diffusion
Kaolinite	$y = -0.0106x + 0.7477$	$y = 0.0214x + 0.0106$	$y = 0.4244x + 42.625$
	$K_1 = 0.024$	$K_2 = 0.043$	$K_i = 0.424$
	$q_e = 5.594$	$q_e = 46.729$	$q_e \cdot exp = 42.625$
Illite	$R^2 = 0.4601$	$R^2 = 0.9999$	$R^2 = 0.5549$
	$y = -0.0132x + 0.7292$	$y = 0.0208x + 0.0102$	$y = 0.4463x + 43.76$
	$K_1 = 0.030$	$K_2 = 0.042$	$K_i = 0.446$
Montmorillonite	$q_e = 5.360$	$q_e = 48.077$	$q_e \cdot exp = 43.76$
	$R^2 = 0.4492$	$R^2 = 0.9999$	$R^2 = 0.6405$
	$y = -0.0106x + 0.789$	$y = 0.0213x + 0.0149$	$y = 0.304x + 43.648$
Montmorillonite	$K_1 = 0.024$	$K_2 = 0.030$	$K_i = 0.024$
	$q_e = 6.162$	$q_e = 46.948$	$q_e \cdot exp = 43.648$
	$R^2 = 0.4402$	$R^2 = 0.9993$	$R^2 = 0.5074$

In Figure 12, the first part of the curve (λ) has a higher slope, indicating adsorption on the outer

surface or stage of penetration into the cortex. The second part of the curve (dr) is the gradual

adsorption or penetration phase of the absorbed material into the holes, which is the rate controlling step due to its lower slope than the previous one. The third step is done very quickly, and is considered minor. In the process design, it is essential to identify the difference between the film penetration and intra-particle penetration in order to identify the slowest step in the adsorption process. The rate of an adsorption process depends on the factors such as the structural properties of the adsorbent including porosity, specific surface area and particle size, chemical properties of the contaminant including ionic radius, contaminant concentration, and the amount of interaction between the dye and the adsorbent.

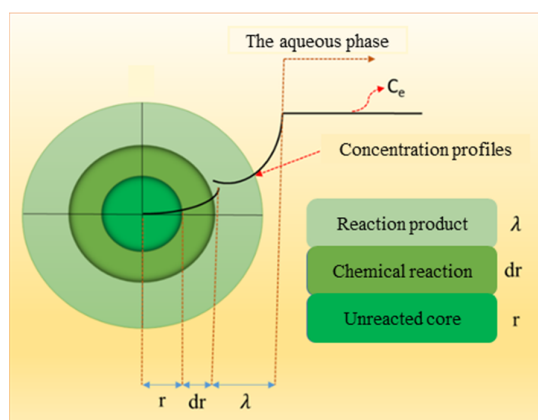


Figure 12. Adsorbed mass transfer and adsorbent concentration profiles [29].

3.8. Adsorption Thermodynamic

Since the adsorption values for MB at the temperatures of 10, 20, 30, and 40 °C were studied

for all the three adsorbents, the values for the thermodynamic parameters can be determined by the Van't Hoff thermodynamic equations.

$$\log K_d = \frac{\Delta S^\circ}{2.303R} - \frac{\Delta H^\circ}{2.303RT} \quad (2)$$

Where ΔS° (Kj/mol.K) is the entropy, ΔH° (KJ/mol) is the enthalpy, R is the gas constant being equal to 8.314 (j/mol.K), and T is the Kelvin temperature. Also K_d is the equilibrium constant, which is obtained from Equation 3.

$$K_d = \frac{a}{1-a} \quad (3)$$

In this equation, a represents the percentage of the pollutant adsorption at equilibrium. The Gibbs free energy of the MB adsorption process is also obtained by Equation 4.

The calculated thermodynamic parameters can be seen in Table 4. The negative ΔG° at the temperatures studied for all the three adsorbents indicate spontaneous adsorption reactions. On the other hand, the enthalpy changes were negative for all the three adsorbents at the studied temperatures, indicating that the adsorptions were exothermic. The small and positive entropy values indicate the low randomness at the solid/solution interface during the adsorption process. Given that both the thermodynamic parameters of enthalpy changes and the entropy change to enhance the reaction, namely exothermic and increasing irregularity, it can be concluded that the positive entropy changes increase, and the positive enthalpy changes decrease the MB adsorption. Thus the adsorption reaction is spontaneous and irreversible.

Table 4. Thermodynamic parameters of MB adsorption.

Adsorbent	ΔH° (KJ/mol)	ΔS° ($\frac{KJ}{mol.K}$)	ΔG° (KJ/mol)			
			Temperature (K)			
			283	293	303	313
Kaolinite	-38.34	0.04	-49.72	-50.15	-50.51	-50.9
Illite	-19.98	0.02	-25.86	-26.09	-26.28	-26.48
montmorillonite	-28.37	0.007	-30.25	-30.32	-30.39	-30.45

One way to determine the type of adsorption is to obtain the amount of adsorption enthalpy. The basis of the work can be divided into two types of adsorption including the physical adsorption and the chemical adsorption. If the enthalpy is less than 20 KJ, it is assumed to be a physical adsorption, and if it is higher than 80 KJ, it is assumed to be a chemical adsorption. According to Table 4, the enthalpy changes for all the three cases are less

than 40 kJ, so all the three adsorption processes can be classified as the physical/partially chemical adsorption categories.

3.9. SEM and FT-IR analysis

In this work, SEM analysis was performed for all the three understudied adsorbent samples. The SEM analysis is shown in Figure 1-S. Although the crushing type was similar for all the three types of

adsorbents, illite had a smaller grain size. In terms of porosity, Figure 1-S shows that the highest porosity is related to illite, followed by montmorillonite with a higher porosity than kaolinite.

One way to identify the adsorption mechanism is to compare the FT-IR spectra before and after the adsorption process. The FT-IR spectra for kaolinite, illite, and montmorillonite before and after MB removal are presented in Figures 14 to 16, respectively. For kaolinite, illite, and montmorillonite, the absorption bands at 1634.72 cm^{-1} , 1637.59 cm^{-1} , and 1634.72 cm^{-1} are ascribed to the $Si-OH$ and $Al-OH$ stretching vibrations in physisorbed water. Above all, the wavenumbers 3399.26 and 3646.40 for illite, 3440.44 cm^{-1} and 3626.41 cm^{-1} for kaolinite, and 3440.44 cm^{-1} and 3626.41 cm^{-1} for montmorillonite show changing; these wavenumbers can be related

to $N-OH$ and $Al-OH$. Therefore, the formation of a bond between the nitrogen present in aqueous methylene and the hydrogens present in the clay structure is shown in Figure 17 [27].

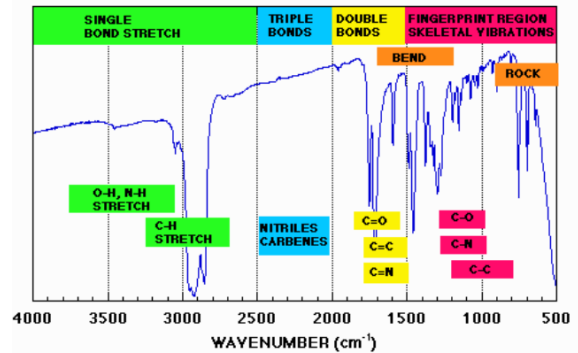


Figure 13. Bond stretch identity graph (www.photometrics.net).

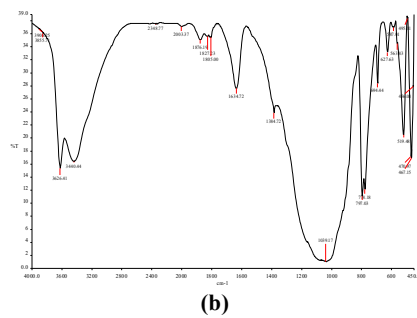
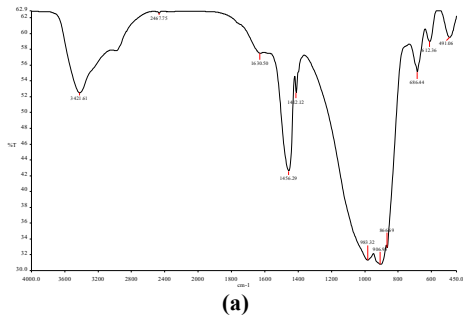


Figure 14. Kaolinite FT-IR spectrum. a: before adsorption, b: after adsorption.

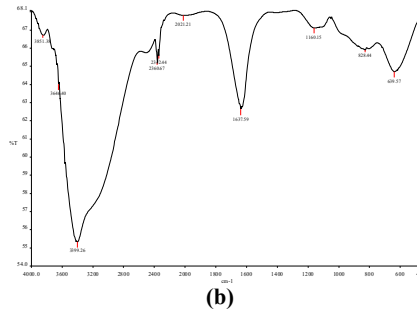
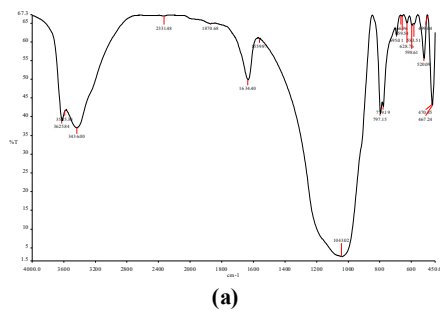


Figure 15. Illite FT-IR spectrum. a: before adsorption, b: after adsorption.

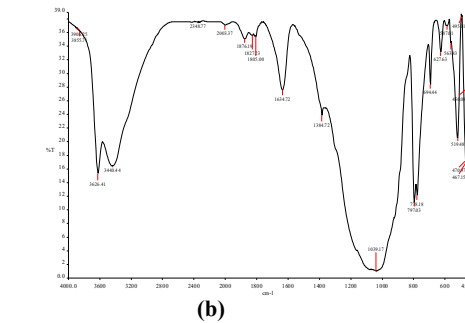
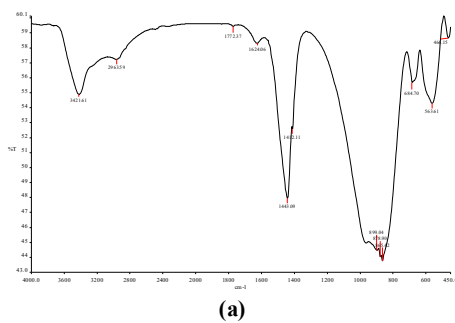


Figure 16. Montmorillonite FT-IR spectrum. a: before adsorption, b: after adsorption.

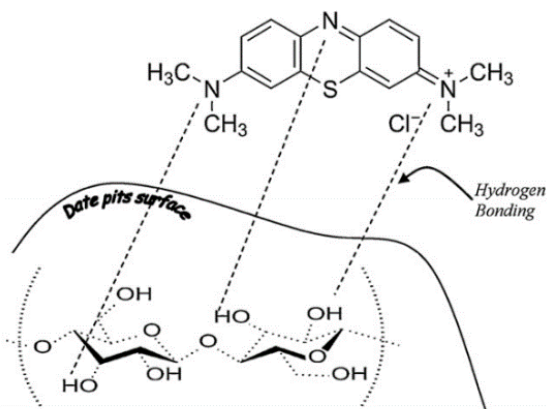


Figure 17. Formation of hydrogen bonds between aqueous methylene and adsorbent [27].

3.10. Molecular modeling

In order to express the relationship between the molecular structures and the rate of physical adsorption, according to the Gaussian and ChemOffice software, the structures of the adsorbents and the MB molecules were simulated, and the information from these software was obtained; Table 4 summarizes some extracted information from the software.

Since in an adsorption, Van der Waals forces and surface electrostatic potential play an important role in the absorption capacity and absorption rate, the modeling of surface electrostatic potential was performed in the Chem3D software (Figure 18).

Table 5. Information extracted from the Gaussian and ChemOffice software.

Parameter	Kaolinite	Illite	Montmorillonite
Connolly accessibly area	414.00	513.4	476.8
Connolly molecular area	229.2	299.3	237.7
Connolly solvent excluded volume	278.69	388.6	354.6
Number of H-bond acceptors	18	24	16
Number of H-bond donors	0	0	0
Orality	1.11	1.16	1.13
Dipole	8.61	9.45	1.15
Molecular topological Index	5956	13832	22416
Polar surface area	140.02	169.28	194.12
Total connectivity	1.50E-06	5.23E-09	5.23E-09
RMS force	66.45	68.95	41.83

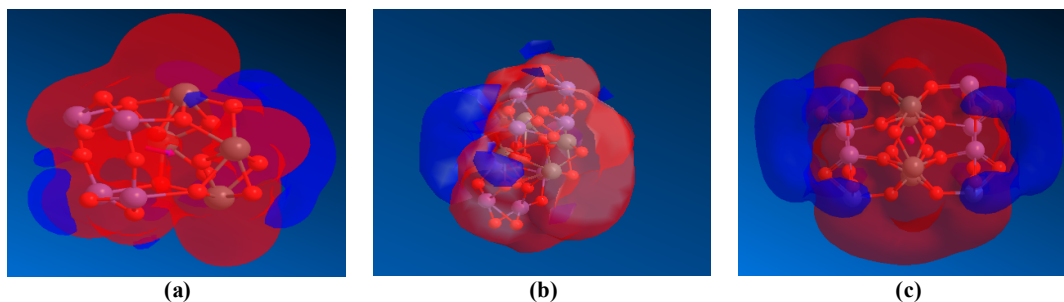


Figure 18. Electrostatic potential modeling of the three clay adsorbents (red color shows a positive electrostatic potential and blue color shows a positive electrostatic potential). a: montmorillonite, b: illite, c: kaolinite.

Considering this figure, it can be seen that montmorillonite has a symmetric electrostatic potential, while the other adsorbents follow an asymmetric shape. All the three adsorbents also have the potential to absorb materials with positive and negative potentials due to the electrostatic properties observed in the Figure 18. In order to illustrate the electrostatic potential of MB, this compound was plotted in the ChemDraw software and the Chem3D software was modeled. Figure 19 shows the electrostatic modeling of MB. In this figure, it is obvious that only the middle nitrogen structure of MB has a positive electrostatic potential.

Based on the results of the FT-IR spectra as well as the molecular modeling, it can be concluded that the intermediate nitrogen is the major contributor to the formation of new N-H bonds in the adsorption process. Thus hydrogen bonds can be considered as the main adsorption factor in the current adsorption processes in this work. According to Table 4 and the number of hydrogen bond acceptors present in each structure, it is expected that the highest adsorption rates are related to illite, kaolinite, and montmorillonite with 24, 18, and 16 hydrogen bond acceptors, respectively. This result is in agreement with the results of the adsorption isotherm.

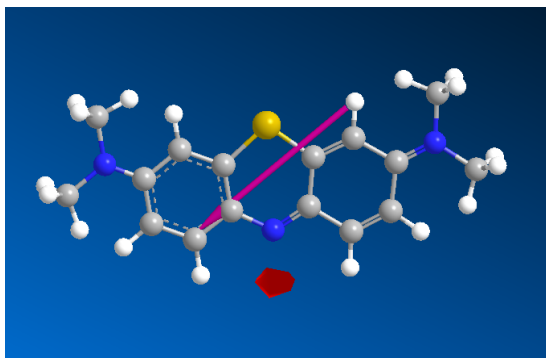


Figure 19. Electrostatic potential of MB (red color indicates a positive potential).

4. Conclusions

Methylene blue (MB) is considered as a main environmental pollutant. In this work, three clays including kaolinite, illite, and montmorillonite from three main clay categories were selected as the adsorbents, and the MB adsorption on these adsorbent were assessed. Initially, the adsorption operating parameters for all the three adsorbents were optimized by the experimental tests and the Design Expert 7 software. Then the adsorption capacity and efficiency of each adsorbent were determined by the adsorption isotherm, and the highest adsorption rate was predicted by the Design Expert 7 software too. All the three adsorbents followed the Temkin isotherm, and the highest adsorption rates were determined for illite, kaolinite, and montmorillonite, respectively. Finally, it was attempted to determine a reasonable relation between the adsorbent structure and its efficiency by molecular modeling and FT-IR analysis. Based on the results obtained, it was assumed that the bond formed between MB and clay was physical. Also the main reason for the adsorption of MB by clays is due to the formation of hydrogen bonds. Of course, the intermediate nitrogen in the MB structure forms a hydrogen bond. Consequently, depending on the number of hydrogen bond acceptors in the structure of each clay, their adsorption might be predicted comparatively.

References

[1]. Mancosu, N., Snyder, R.L., Kyriakakis, G. and Spano, D., 2015. Water scarcity and future challenges for food production. *Water*. 7 (3): pp.975-992.

[2]. Lazaratou, C.V., Vayenas, D.V. and Papoulis, D. (2020). The role of clays, clay minerals and clay-based materials for nitrate removal from water systems: A review. *Applied Clay Science*, 185, p.105377.

[3]. Wang, R.C., Fan, K.S. and Chang, J.S., 2009. Removal of acid dye by ZnFe₂O₄/TiO₂-immobilized granular activated carbon under visible light irradiation in a recycle liquid–solid fluidized bed. *Journal of the Taiwan Institute of Chemical Engineers*. 40 (5): pp.533-540.

[4]. Chen, H., Luo, H., Lan, Y., Dong, T., Hu, B. and Wang, Y. (2011). Removal of tetracycline from aqueous solutions using polyvinylpyrrolidone (PVP-K30) modified nanoscale zero valent iron. *Journal of hazardous materials*. 192 (1): pp.44-53.

[5]. Xia, L., Zhou, S., Zhang, C., Fu, Z., Wang, A., Zhang, Q., Wang, Y., Liu, X., Wang, X. and Xu, W. (2020). Environment-friendly *Juncus effusus*-based adsorbent with a three-dimensional network structure for highly efficient removal of dyes from wastewater. *Journal of Cleaner Production*, p.120812.

[6]. Dutta, A.K., Maji, S.K. and Adhikary, B. (2014). γ -Fe₂O₃ nanoparticles: An easily recoverable effective photo-catalyst for the degradation of rose bengal and methylene blue dyes in the waste-water treatment plant. *Materials Research Bulletin*, 49, pp.28-34.

[7]. Arfi, R.B., Karoui, S., Mougin, K. and Ghorbal, A. (2017). Adsorptive removal of cationic and anionic dyes from aqueous solution by utilizing almond shell as bioadsorbent. *Euro-Mediterranean Journal for Environmental Integration*. 2 (1): p.20.

[8]. Hou, Y., Yan, S., Huang, G., Yang, Q., Huang, S. and Cai, J. (2020). Fabrication of N-doped carbons from waste bamboo shoot shell with high removal efficiency of organic dyes from water. *Bioresource Technology*. 303: p.122939.

[9]. Kurmarayuni, C.M., Kurapati, S., Akhil, S., Chandu, B., Khandapu, B.M.K., Koya, P.R. and Bollikolla, H.B. (2020). Synthesis of multifunctional graphene exhibiting excellent sonochemical dye removal activity, green and regioselective reduction of cinnamaldehyde. *Materials Letters*. 263: p.127224.

[10]. Gupta, V.K., Carrott, P.J.M., Ribeiro Carrott, M.M.L. and Suhas. (2009). Low-cost adsorbents: growing approach to wastewater treatment a review. *Critical reviews in environmental science and technology*. 39 (10): pp.783-842.

[11]. Seow, W.Y. and Hauser, C.A., 2016. Freeze-dried agarose gels: A cheap, simple and recyclable adsorbent for the purification of methylene blue from industrial wastewater. *Journal of environmental chemical engineering*. 4 (2): pp.1714-1721.

[12]. Januário, Eduarda Freitas Diogo, Natália de Camargo Lima Beluci, Taynara Basso Vidovix, Marcelo Fernandes Vieira, Rosângela Bergamasco, and Angélica Marquetotti Salcedo Vieira. (2020). 'Functionalization of membrane surface by layer-by-layer self-assembly method for dyes removal', *Process Safety and Environmental Protection*. 134: 140-48.

- [13]. Siboni, M.S., Samarghandi, M., Yang, J.K. and Lee, S.M. (2011). Photocatalytic removal of reactive black-5 dye from aqueous solution by UV irradiation in aqueous TiO₂: equilibrium and kinetics study. *J. Adv. Oxid. Technol*, 14, pp.302-307.
- [14]. Abbasi, M. and Asl, N.R. (2008). Sonochemical degradation of Basic Blue 41 dye assisted by nanoTiO₂ and H₂O₂. *Journal of hazardous materials*. 153 (3): pp.942-947.
- [15]. Ouni, H. and Dhahbi, M. (2010). Removal of dyes from wastewater using polyelectrolyte enhanced ultrafiltration (PEUF). *Desalination and Water Treatment*: 22 (1-3): pp.355-362.
- [16]. Clematis, D., Cerisola, G. and Panizza, M. (2017). Electrochemical oxidation of a synthetic dye using a BDD anode with a solid polymer electrolyte. *Electrochemistry Communications*, 75, pp.21-24.
- [17]. García-Montaño, J., Pérez-Estrada, L., Oller, I., Maldonado, M.I., Torrades, F. and Peral, J., 2008. Pilot plant scale reactive dyes degradation by solar photo-Fenton and biological processes. *Journal of Photochemistry and Photobiology A: Chemistry*. 195 (2-3): pp.205-214.
- [18]. Sahinkaya, E., Sahin, A., Yurtsever, A. and Kitis, M., 2018. Concentrate minimization and water recovery enhancement using pellet precipitator in a reverse osmosis process treating textile wastewater. *Journal of environmental management*, 222, pp.420-427.
- [19]. Srinivasan, A. and Viraraghavan, T. (2010). Decolorization of dye wastewaters by biosorbents: a review. *Journal of environmental management*. 91 (10): pp.1915-1929.
- [20]. Li, R., Wang, J.J., Zhou, B., Awasthi, M.K., Ali, A., Zhang, Z., Gaston, L.A., Lahori, A.H. and Mahar, A., 2016. Enhancing phosphate adsorption by Mg/Al layered double hydroxide functionalized biochar with different Mg/Al ratios. *Science of the Total Environment*. 559: pp.121-129.
- [21]. Anastopoulos, Ioannis, Ahmad Hosseini-Bandegharai, Jie Fu, Athanasios C Mitropoulos, and George Z Kyzas. (2018). 'Use of nanoparticles for dye adsorption', *Journal of Dispersion Science and Technology*, 39: 836-47.
- [22]. Rai, P., Gautam, R.K., Banerjee, S., Rawat, V. and Chattopadhyaya, M.C. (2015). Synthesis and characterization of a novel activated carbon magnetic nanocomposite and its effectiveness in the removal of crystal violet from aqueous solution. *Journal of Environmental Chemical Engineering*. 3 (4): pp.2281-2291.
- [23]. Rahman, M.A., Amin, S.R. and Alam, A.S. (2012). Removal of methylene blue from waste water using activated carbon prepared from rice husk. *Dhaka University Journal of Science*. 60 (2): pp.185-189.
- [24]. Omer, O.S., Hussein, M.A., Hussein, B.H. and Mgaidi, A., 2018. Adsorption thermodynamics of cationic dyes (methylene blue and crystal violet) to a natural clay mineral from aqueous solution between 293.15 and 323.15 K. *Arabian Journal of Chemistry*. 11 (5): pp.615-623.
- [25]. Ayawei, Nimibofa, Augustus Newton Ebelegi, and Donbebe Wankasi. (2017). 'Modelling and interpretation of adsorption isotherms', *Journal of Chemistry*, 2017.
- [26]. Bandar, S., Anbia, M. and Salehi, S., Comparison of MnO₂ modified and unmodified magnetic Fe₃O₄ nanoparticle adsorbents and their potential to remove iron and manganese from aqueous media. *Journal of Alloys and Compounds*, 851, p.156822.
- [27]. Al-Ghouti, M.A., Li, J., Salamh, Y., Al-Laqtah, N., Walker, G. and Ahmad, M.N. (2010). Adsorption mechanisms of removing heavy metals and dyes from aqueous solution using date pits solid adsorbent. *Journal of hazardous materials*. 176 (1-3): pp.510-520.
- [28]. Shabani, K.S., Ardejani, F.D., Badii, K. and Olya, M.E. (2017). Preparation and characterization of novel nano-mineral for the removal of several heavy metals from aqueous solution: Batch and continuous systems. *Arabian Journal of Chemistry*, 10, pp.S3108-S3127.
- [29]. Ko, D.C., Porter, J.F. and McKay, G. (2001). Film-pore diffusion model for the fixed-bed sorption of copper and cadmium ions onto bone char. *Water research*. 35 (16): pp.3876-3886.

مطالعات آزمایشگاهی، روش سطح پاسخ و مدل سازی مولکولی به منظور تحلیل مکانیسم و بهینه سازی حذف رنگزای متیل آبی با استفاده از رس های مختلف

کیومرث سیف پناهی شعبانی* و بابک عابدی اورنگ

دانشکده مهندسی معدن، نفت و ژئوفیزیک، دانشگاه صنعتی شاهرود، شاهرود، ایران

ارسال ۲۰۲۰/۰۷/۲۲، پذیرش ۲۰۲۰/۰۹/۱۹

* نویسنده مسئول مکاتبات: seifpanahi@shahroodut.ac.ir

چکیده:

در این مقاله سه نوع رس های طبیعی دارای ساختارهای مختلف شامل کائولینیت، مونتوریلونیت و ایلیت به عنوان جاذب هایی برای حذف رنگزای متیل آبی انتخاب شده و کارایی آنها بررسی شده است. همچنین بهینه سازی و تحلیل مکانیسم جذب رنگزا با استفاده از روش سطح پاسخ، مدل سازی مولکولی و داده های آزمایشگاهی بررسی شده است. نتایج بهینه سازی به روش سطح پاسخ نشان می دهد پارامترهای آزمایشگاهی تاثیرگذار بر فرآیند جذب سطحی رنگزا در سه نوع رس مشابه است و پارامتر خاصی برای نوع خاصی از ساختار رسی مطرح نیست. نتایج بررسی های آزمایشگاهی نشان می دهد که هر سه نوع رس از ایزوترم تمکین تبعیت می کنند و مقایسه ظرفیت جذب سه نوع رس به صورت ایلیت (۳/۲۸) > کائولینیت (۴/۱۵) > مونتوریلونیت (۴/۵) لیتر در گرم است. همچنین نتایج دیگری از مطالعات آزمایشگاهی، بهینه سازی به روش سطح پاسخ و مدل سازی مولکولی با استفاده از نرم افزار گوسین و کم آفیس بدست آمده است. نتایج این دست آوردها تایید می کند که تعدادی از پیوندهای پذیرنده هیدروژن در اطراف رس ها بر روی ظرفیت جذب رنگزای متیل آبی توسط این جاذب ها موثر است. بر مبنای نتایج، ظرفیت جذب رس ها به صورت ایلیت < کائولینیت < مونتوریلونیت است که هرکدام به ترتیب ۲۴، ۱۸ و ۱۶ اتم پذیرنده هیدروژن دارند. ارزیابی مکانیسم فرآیند جذب با استفاده از روش های مختلف نشان می دهد که فرآیند جذب فیزیک غالب است و به صورت جزئی و ناچیز فرآیند جذب شیمیایی وجود دارد.

کلمات کلیدی: جذب سطحی، متیل آبی، روش سطح پاسخ، مدل سازی مولکولی.